Eur. Phys. J. B **29**, 503–509 (2002)
DOI: 10.1140/epjb/e2002-00332-5

THE EUROPEAN PHYSICAL JOURNAL B

Induced bubble shape oscillations and their impact on the rise velocity

J. de Vries, S. Luther, and D. Lohse[a]

Department of Applied Physics and J. M. Burgers Centre for Fluid Dynamics, University of Twente, 7500 AE Enschede, The Netherlands

Received 9 April 2002 / Received in final form 11 July 2002
Published online 14 October 2002 –

Abstract. When a 2–4 mm diameter bubble rising with constant velocity hits a thin wire, bubble shape oscillations can be induced. As a consequence also the bubble rise velocity strongly oscillates. With the help of a force balance we show that these velocity oscillations are an added-mass effect.

PACS. 47.55.Dz Drops and bubbles – 47.20.Dr Surface-tension-driven instability

1 Introduction

What is the impact of a bubble's shape oscillation on its rise velocity? Recent experiments by Wu and Gharib [1] with rising bubbles in still water suggest that an oscillating bubble can be nearly twice as fast as an non-oscillating bubble of the same volume. Bubbles with equivalent diameters (*i.e.*, the diameter of a spherical bubble of the same volume) ranging from $d_e = 1-2$ mm were analyzed. Whether the bubble was in the shape oscillating mode or in the non-oscillating mode depended on the way how it was generated: The *non-oscillating, slow* bubble was generated using a *large* capillary $d_{capillary} \sim d_e$ and its velocity was comparable to the rise velocity of a solid sphere of the same volume [2]. The *shape oscillating, fast* bubble (with the same volume) was generated using a *narrow* capillary $d_{capillary} \ll d_e$ and its mean velocity was only slightly slower than that predicted for a clean bubble with slip boundary conditions [2]. Wu and Gharib [1] conclude that there are two different "modes" for rising bubbles. Depending on the way of bubble generation, they end up either in the fast or in the slow mode.

The Wu and Gharib results [1] are very surprising and had not been found in previous experiments. *e.g.* Duineveld [3,4], Maxworthy *et al.* [5], and de Vries [6] all find fast non-oscillating bubbles, close to the theoretical velocities predicted for slip boundary conditions. These researchers also all stress the important role of the surfactants on the bubble's rise velocity which slow them down. The reason for this is that the boundary conditions on the bubbles are (partly) modified to no-slip boundary conditions. However, in these analyses the impact of the bubble shape oscillations on the rise velocity has not been studied.

The only study known to us which is studying the interplay between bubble shape oscillations and the bubble velocity is the study by Lunde and Perkins [7]. These authors analyzed rising bubbles with an equivalent diameter $d_e = 2.4-5.0$ mm in tap water, corresponding to Weber numbers between $We = 3.6-4.3$. Undamped bubble shape and velocity oscillations were observed, starting immediately after bubble detachment from the nozzle. From the oscillating bubble shape the time dependent added-mass force on the bubble was extracted. The corresponding bubble acceleration was in reasonable agreement with what was found through a data analysis of the bubble's path. Drag and buoyancy were not considered in that analysis.

The analyses of references [1,7] are in contrast to the recent results by Ellingsen and Risso [8], also obtained for tap water: Though their $d_e = 2.5$ mm bubble was produced with a *narrow* capillary (inner diameter 0.33 mm $\ll d_e$), these authors did not observe bubble shape oscillations, but an instability of the bubble's path [6,9,10]. The *absolute value* of the velocity was constant, but the *direction* was oscillating. These oscillations were connected to the observed zigzagging or spiraling of the bubbles [6,10,11].

To clarify how bubble shape oscillations affect the rise velocity, it is desirable to study the very same bubble in the same water (guaranteeing the same amount and kind of surfactants), *once without* and *once with* shape oscillations. This can be achieved by letting a rising non-oscillating bubble hit a wire and induce shape oscillations this way. The results on such experiments are reported in this paper.

These type of experiments also offer the opportunity to study the hydrodynamic forces on a bubble, in particular the added-mass force and the drag force. These forces

[a] e-mail: lohse@tn.utwente.nl

are crucial to control bubbles in flow situations. Though considerable progress had been achieved [12,13,11,14], these forces are still not fully understood. In particular, little is known on how bubble shape oscillations affect them. We will construct a simple force balance model to theoretically account for our findings.

We mention that the starting point of our studies had been hot-film anemometry in turbulent bubbly flow [15]. In order to better understand the interaction between the hot-film anemometer probe and a passing bubble, we employed high speed cinematography correlating the image sequences with the probe signal. The results from that study will be reported elsewhere [16].

The outline of the present paper is as follows: In Section 2 the experiment and its results are described. In Section 3 the approximate force balance model for the rising shape-oscillating bubble is derived, whose results for the oscillating bubble velocity are compared with direct measurements in Section 4. The paper ends with a summary and an estimate about what will happen for smaller bubbles (Sect. 5).

2 Experiments

The experiments were performed in ultra-clean (purified) water comparable to the water used by Duineveld [3]. The bubbles were released from a capillary with inner diameter of 1.0 mm. The bubble volume was controlled through the gas flow rate. The typical equivalent diameter was $d_e = 2.0 - 4.0$ mm. We used a stereoscopic setup and a high-speed camera (2000 fps) to measure the shape and the velocity of the bubble before, during, and after the bubble hits a hot-film anemometer. From each frame of the sequence of stereo image pairs the bubble's centroid and contour were obtained. From the contour line several shape descriptors as well as the eccentricity and the major and minor axes were measured. The accuracy of the measurement of the position of the bubble is typically ± 200 μm. The three dimensional trajectory of the rising bubble was obtained by tracking the bubbles with a Kalman filter [17,18]. Thus, an estimate of the position and velocity of the bubble was obtained.

For a bubble with $d_e = 2.4$ mm the rise velocity v relative to the liquid was 0.33 ms^{-1}, corresponding to a Weber number of $We = \rho_l v^2 d_e \sigma_l^{-1} = 3.6$. Here, ρ_l and σ_l denote the density and the surface tension of the liquid, respectively. Note that the rise velocities of a $d_e = 2.4$ mm bubble reported by Clift *et al.* [2], Maxworthy *et al.* [5], and Ellingsen and Risso [8] are slightly lower, namely 0.28 ms^{-1} and 0.31 ms^{-1}, respectively. This presumably is due to a slight contamination of their water, as extensively discussed by *e.g.* Duineveld [3,4].

The interaction of the bubbles with the probe (cylindrical and 74 μm in diameter) can induce bubble shape oscillations, which cause also an oscillation of the rise velocity. Figure 1 shows images recorded with the high-speed camera after the interaction with the hot-film probe. The velocity of the bubble before, during and after the interaction is given in Figure 2. Figure 3 presents the three

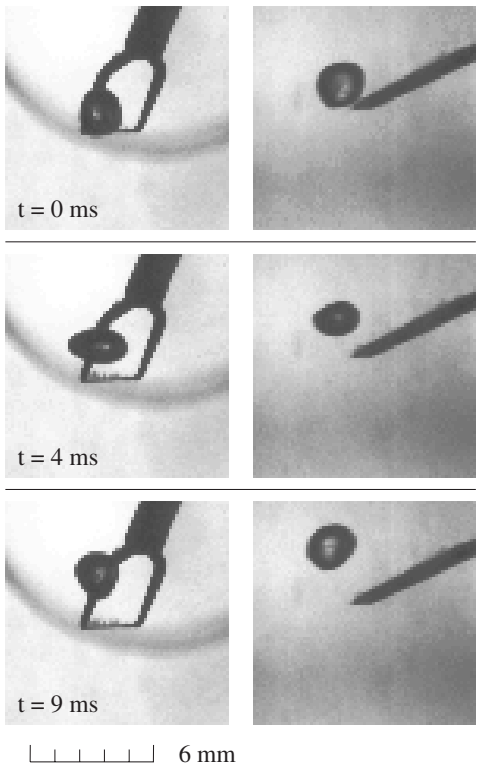

Fig. 1. Selected frames of a sequence of the high-speed images. In the left frame the bubble and the hot-film probe are shown. In the right frame the same bubble and probe are shown, but from a direction turned by 90°. The view in the right frame is corresponding to the view from the right side in the left frame. The equivalent bubble diameter is $d_e = 2.4$ mm. The given times correspond to the marked times of Figure 2. The bubble detaches from the probe at $t = 0$ s.

axes a, b, and c (defined in Fig. 4) of the bubble also before, during and after the interaction. The oscillations of the axes have the same period as the oscillation of the velocity. From Figures 2 and 3 it is clear that the bubble's shape and velocity do not oscillate before the interaction. The oscillations are induced by the interaction with the probe. During the inelastic collision the bubble loses momentum thus reducing its mean rise velocity. As the bubble departs from the wire, the mean velocity increases again towards its asymptotic limit. In contrast to the findings of reference [1], no increase of the mean velocity of the now oscillating bubble is observed.

Let us now account for the frequency of the observed bubble shape oscillations. For the $d_e = 2.4$ mm bubble shown in Figures 1–3, the period of the shape and the velocity oscillations is 9 ± 1 ms. In Table 1 the values for bubbles with various diameters are given. How do these measured frequencies agree with the expected value for bubble shape oscillations? This theoretical frequency is given by [19]

$$\omega_n^2 = \frac{\beta_n \sigma_l}{\rho_l (\frac{1}{2} d_e)^3}, \qquad (1)$$

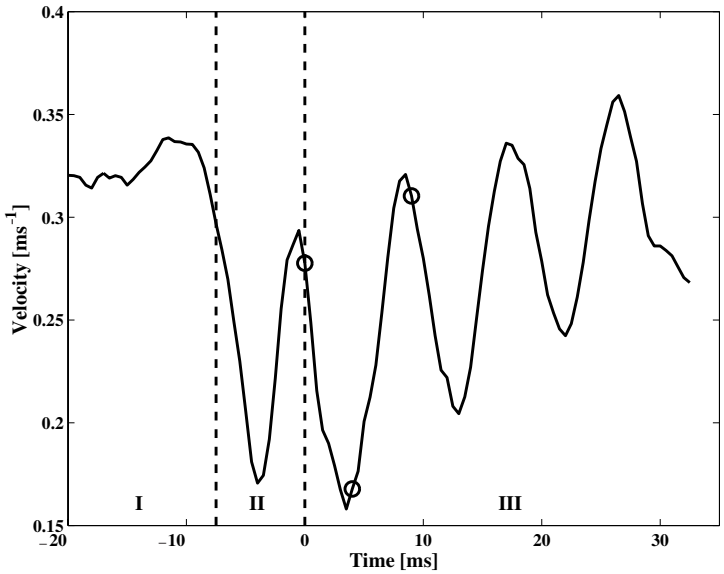

Fig. 2. The measured velocity v_z of a rising bubble. The regions I, II, and III denote the bubble's approach, collision, and departure, respectively. The bubble departs from the probe with collision induced velocity oscillations. The circles correspond to the frames depicted in Figure 1.

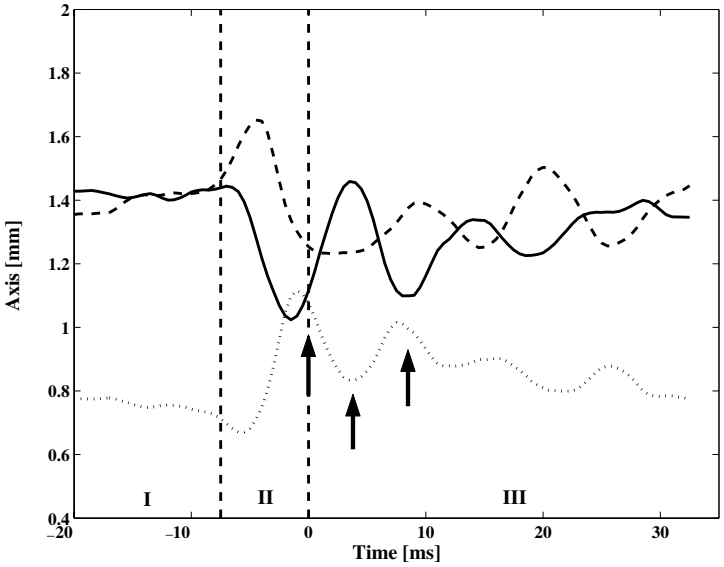

Fig. 3. The experimental determined axes a and b (solid and dashed) and c (dotted) of a rising bubble. For $t < -10$ ms the bubble axes are constant within experimental errors. At $t = -7.5$ ms the interaction between the bubble and the hot-film probe starts. At $t = 0$ s the bubble detaches from the hot-film probe and its axes oscillate. The arrows are drawn at the times $t = 0$ ms, 4 ms, and 9 ms shown in Figure 1.

with $\beta_n = (n-1)(n+1)(n+2)$. From looking at the image frames we find $n = 2$. For the $d_e = 2.4$ mm bubble of Figures 1–3 the theoretical period $T = 2\pi/\omega = 1/f$ is $T = 8.8$ ms, in very good agreement with the measured value of 9 ± 1 ms (from Figs. 2, 3). In Table 1 a comparison of the theoretical and experimental periods of various oscillating bubbles are given. It shows good agreement within the accuracy of the measurement, which is given as $\Delta T_{exp} \approx 1 - 2$ ms in the last column of the table.

3 Force balance

Now we describe the equation of motion for the bubble using a force balance model. We consider the rise of the bubbles in quiescent uncontaminated water, *i.e.* there is no shear stress between bubble and liquid. The sum of the forces acting on the bubble results in a change of momentum of the bubble,

$$\sum \mathbf{F} = \mathbf{F}_b + \mathbf{F}_d + \mathbf{F}_a = \frac{\mathrm{d}}{\mathrm{d}t}(m\mathbf{v}) \approx 0 \qquad (2)$$

Table 1. A comparison between the theoretical and the experimental values of the period T of shape oscillations of various oscillating bubbles with different d_e. The theoretical values refer to the $n = 2$ mode which is the one observed in the experiments. Also given are the bubble rise velocities before the impact on the wire and the corresponding Weber numbers $We = \rho_l v^2 d_e \sigma_l^{-1}$.

d_e [mm]	v [m s^{-1}]	We	T_{theory} [ms]	$T_{exp} \pm \Delta T_{exp}$ [ms]
2.2	0.30	2.7	7.7	9 ± 1
2.4	0.33	3.6	8.8	9 ± 1
2.6	0.30	3.2	9.6	10 ± 1
2.8	0.31	3.7	11.1	14 ± 2
3.2	0.28	3.4	13.6	14 ± 2

where $m = \rho_g V_b$ is the mass of the gas bubble with density ρ_g and volume V_b, and $\mathbf{v}$ its the velocity relative to the fluid. The mass of the bubble can be neglected, as $\rho_l \gg \rho_g$ for the liquid density. The forces acting on the bubble are the buoyancy force $\mathbf{F}_b$, the drag force $\mathbf{F}_d$, and the added-mass force $\mathbf{F}_a$, which is an inertia effect originating from the necessity for the rising bubble to push the water away. We assume that there is no history force. Moreover, there is no lift force as the water is at rest. An extensive discussion of all forces can be found in reference [20].

The buoyancy force is

$$\mathbf{F}_b = \rho_l V_b \mathbf{g}, \tag{3}$$

where $\mathbf{g} = (0, 0, g)$ is the gravitational acceleration.

The drag force is

$$\mathbf{F}_d = -\frac{1}{2} C_d \rho_l \pi R_s^2 |\mathbf{v}| \mathbf{v}, \tag{4}$$

where πR_s^2 is the area of the bubble projected onto a plane perpendicular to the direction of motion. The drag coefficient C_d depends both on the Reynolds number and the shape of the bubble. We assume that the shape of the bubble can be approximated by an oblate axisymmetrical ellipsoid. If we denote the principal axes of the ellipsoid with a, b, and c, this assumption corresponds to $a = b \geq c$ (see Fig. 4). Furthermore, we assume that the bubble moves along its axis of symmetry, *i.e.* its minor axis. Then the drag coefficient C_d is given by [21]

$$C_d = \frac{48}{Re} G(\epsilon) \left(1 + \frac{H(\epsilon)}{\sqrt{Re}}\right), \tag{5}$$

where the eccentricity is defined by $\epsilon = a/c = b/c \geq 1$. The Reynolds number is defined as $Re = 2R_s|\mathbf{v}|\nu_l^{-1}$ with ν_l denoting the liquid viscosity. The shape dependence of the drag coefficient C_d is captured by the functions $G(\epsilon)$ and $H(\epsilon)$. For the bubbles analyzed in this paper the Reynolds number is 800 and above. Therefore, and as $|H(\epsilon)|$ is order of 1, the second term on the right-hand side in equation (5) can be neglected. Thus, we restrict our description to first order corrections. The shape factor $G(\epsilon)$ can be expressed through [21]

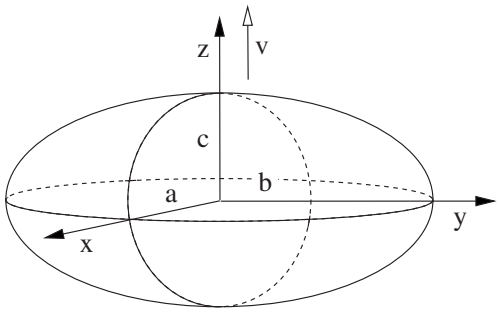

Fig. 4. Definition of the axes a, b, and c for an ellipsoidal bubble moving with the velocity $\mathbf{v}$ relative to the liquid. The bubble is called oblate (prolate), if $a, b > c$ ($a, b < c$).

$$G(\epsilon) = \frac{1}{3}\epsilon^{4/3}(\epsilon^2 - 1)^{3/2} \frac{[(\epsilon^2 - 1)^{1/2} - (2 - \epsilon^2)\sec^{-1}\epsilon]}{[\epsilon^2 \sec^{-1}\epsilon - (\epsilon^2 - 1)^{1/2}]^2}. \tag{6}$$

For a spherical bubble $\epsilon = 1$ and $G = 1$. With increasing ϵ also G increases rapidly. Therefore, a bubble of given volume will experience an increased drag if its surface is distorted.

The most relevant force in our context here will turn out to be the added-mass force. It is given by

$$\mathbf{F}_a = -\frac{\mathrm{d}}{\mathrm{d}t}(\underline{\mathbf{M}}\mathbf{v}), \tag{7}$$

where $\underline{\mathbf{M}}$ denotes the added-mass tensor, which is derived in articles 114, 115, and 121 of Lamb [19]. Note that in general the velocity change and the added mass force need not be parallel. Here, however, for simplicity we make two approximations: (i) Again, we assume that the bubble is an oblate axisymmetric ellipsoid. (ii) We assume that its symmetry axis is the z-axis in the laboratory frame. From Figures 1 and 3 (and from unshown material) we see that these approximations are delicate directly after the bubble's detachment from the wire. However, the point we want to make turns out to be robust, and therefore we feel free to use the approximation. Employing (i) and (ii) and restricting ourselves to the z-component of the velocity leaves us with

$$M_{zz} = \rho_l V_b \frac{\gamma_0}{2 - \gamma_0} \tag{8}$$

as only relevant part of the added mass tensor, with

$$\gamma_0 = \frac{2}{e^2}\left(1 - \frac{\sqrt{1 - e^2}}{e}\arcsin(e)\right), \tag{9}$$

$e = \sqrt{1 - (c/a)^2} = \sqrt{1 - (c/b)^2} = \sqrt{1 - \epsilon^{-2}}$. For a spherical bubble $e = 0$, $\gamma_0 = 2/3$, and we recover the well known result that the added mass is $\rho_l V_b/2$.

Inserting equations (3–8) in equation (2) yields the force balance

$$0 = \rho_l V_b g - \frac{1}{2} C_d \rho_l \pi R_s^2 |v_z| v_z - \frac{\mathrm{d}}{\mathrm{d}t}(M_{zz} v_z). \tag{10}$$

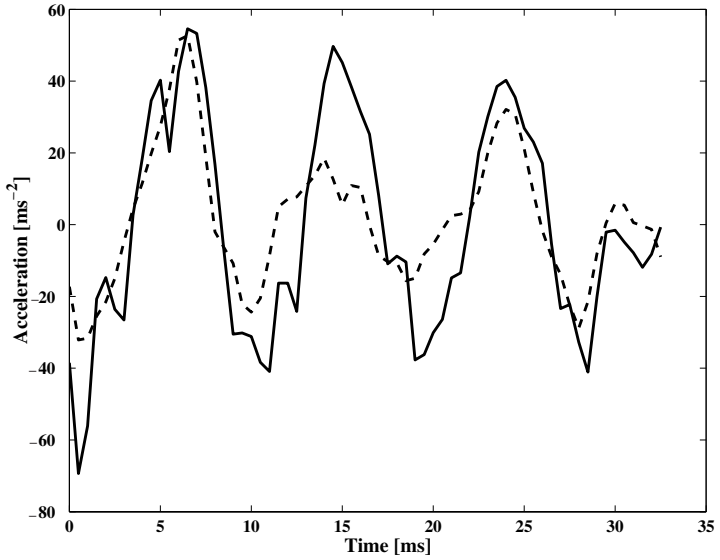

Fig. 5. The experimental (solid) and numerically calculated (dashed) acceleration $\mathrm{d}v_z/\mathrm{d}t$ of the bubble.

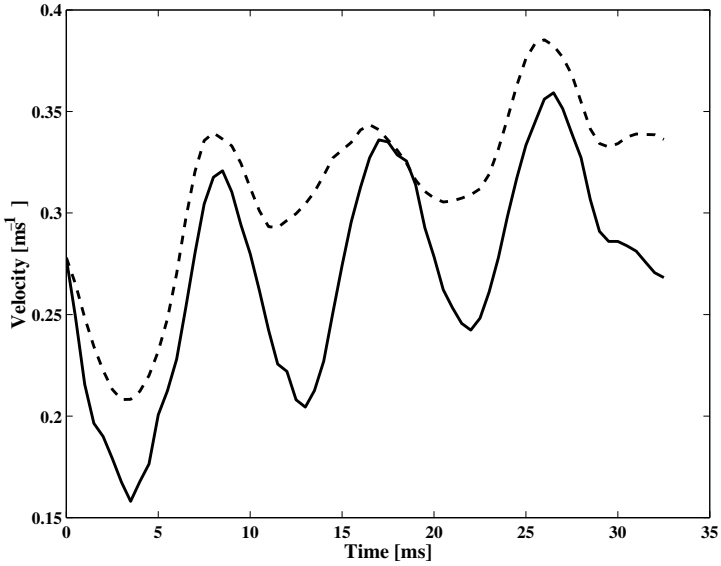

Fig. 6. The experimental (solid) and numerically calculated (dashed) velocity v_z of the bubble.

Note that both the drag coefficient and the added-mass are time dependent, *i.e.* $C_d = C_d(t)$ and $M_{zz} = M_{zz}(t)$, respectively. Considering this, equation (10) can be rewritten as

$$M_{zz}(t)\frac{\mathrm{d}}{\mathrm{d}t}v_z(t) = \rho_l V_b g - \frac{1}{2}C_d(t)\rho_l \pi R_s(t)^2 |v_z(t)| v_z(t) - v_z(t)\frac{\mathrm{d}}{\mathrm{d}t}M_{zz}(t). \quad (11)$$

We solve this ODE with a fourth-order Runge-Kutta scheme. From the experimental data we obtain the principal axes of the bubble $a = a(t)$, $b = b(t)$, and $c = c(t)$ as described in Section 2 (see Fig. 3). The drag coefficient $C_d(t)$ and the added-mass coefficient $M_{zz}(t)$ are then computed with equations (5, 6) and equations (8, 9), respectively. The experimental data is available at discrete time steps only. Therefore interpolation with cubic splines provides intermediate values required for the numerical calculation. The initial conditions and the parameters values for the numerical simulation of equation (11) are as follows. The initial velocity of the bubble at $t = 0$ ms, *i.e.* at the detachment of the bubble from the probe, is $v(0) = 0.28$ m s^{-1}. The bubble's volume is assumed to be constant with $V_b = 6.3$ mm^3. The gravitational acceleration, the density, and viscosity of the liquid are $g = 9.81$ m s^{-2}, $\rho_l = 998$ kg m^{-3}, and $\nu_l = 10^{-6}$ m^2 s^{-1}, respectively.

4 Comparison between the model and experimental data

In Figures 5 and 6 the experimental and numerical accelerations and velocities are shown. From Figures 5 and 6

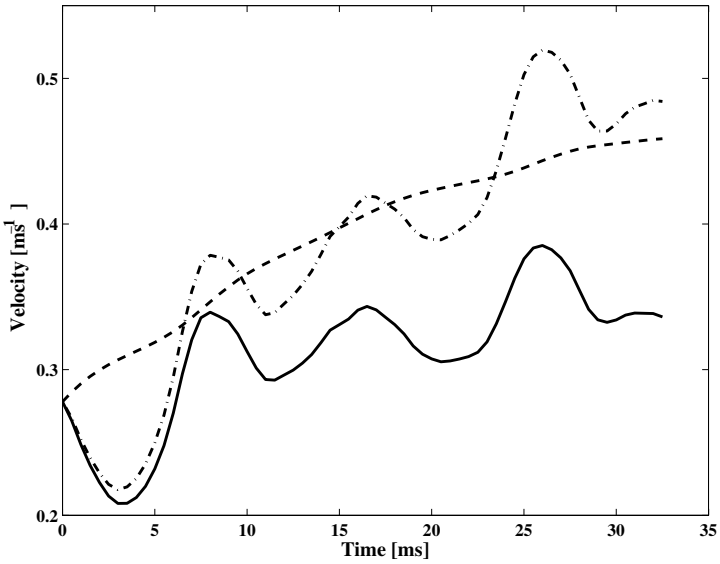

Fig. 7. The numerically calculated velocities v_z of the bubble. The solid line corresponds to the full numerical model, *i.e.*, $\mathbf{F_b}$, $\mathbf{F_d}$ and $\mathbf{F_a}$ of equation (2). For the dashed line only $\mathbf{F_b}$ and $\mathbf{F_d}$ have been employed; that curve shows only very small oscillations. For the dashed-dotted curve only $\mathbf{F_b}$ and $\mathbf{F_a}$ have been employed; that curve shows strong velocity oscillations.

it is clear that the frequencies of the shape oscillations of the experimental and numerical data agree very well. Also the amplitude for the acceleration agrees reasonably, at least during the first and third period. During the second period (10–23 ms) the agreement in the acceleration is only qualitative. Our interpretation of this quantitative disagreement is as follows: From Figure 3 it can be seen that in that time interval the amplitude of the minor axis c is a bit suppressed. Probably this is an artifact due to the assumptions that are made in analyzing the images. Because of the smaller amplitude of the oscillations of the minor axis, also the amplitude of the calculated velocity oscillations will be smaller. Another difference is that the mean value of the velocity is about 20% larger in the numerical data than in the experimental data. Ellingsen and Risso [8] predict an increase of the drag by the instability of the wake behind the bubble in a non-rectilinear path. As this instability is not reflected in the model, it can be a further origin of the smaller mean velocity in the experimental case. Further reasons for the quantitative discrepancy can be the employed approximations for the added mass tensor $\underline{\mathbf{M}}$, the (neglected) added-mass force needed for the *rotation* of the ellipsoidal bubble, or the back reaction on the bubble of the flow induced by the shape oscillations.

We now want to study whether it is the shape oscillation induced oscillation in the drag or in the added-mass force in equation (10) which is responsible for the velocity fluctuations. Therefore we turn off various forces in equation (10) and repeat the numerical integration. The result is shown in Figure 7. Including only buoyancy and the drag force results in an increase of the velocity, and in very small oscillations. In fact that the velocity increases shows that we underestimate the drag, as compared to experiment. The calculations are done with the no-slip drag coefficient, whereas tiny contaminations of the water will lead to a larger drag coefficient and correspondingly to less acceleration and a smaller equilibrium rise velocity. When the added-mass force is included in the force balance (so all forces are included now), the velocity is further decreased and it starts to oscillate with an amplitude that is much larger than the oscillations caused by the drag force. So we have demonstrated that the oscillations in the velocity are *due to the oscillating added-mass force*, and not to the oscillating drag force.

This also reflects in the relative phases of the maxima and minima of the bubble axes and the velocities. When the vertical bubble extension c is minimal (roughly at $t =$ 4 ms, 12 ms, and 22 ms in Fig. 3), the horizontal extension $\sqrt{ab}$ gets maximal and therefore also the amount of water the bubble has to push. Correspondingly, at those times the bubble's acceleration (Fig. 5) gets minimal and slightly later therefore the bubble's velocity (Fig. 6).

The most relevant difference between our results and those from Lunde and Perkins [7] is the way how the oscillations arise. Whereas Lunde and Perkins observe *spontaneous* bubble oscillations because they use narrow capillaries, we *induce* oscillations through the interaction between the bubble and the probe and are thus able to observe the *very same bubble* either oscillating or not. A quantitative comparison also shows that in our case the amplitude of the oscillation of the major and minor axes is about three times larger. Also the acceleration of the bubbles (Fig. 5) is larger in our experiments, about seven times. Another difference is the damping of the oscillations. Whereas the oscillations in our experiments are damped, those in the experiments by Lunde and Perkins are not. As the bubbles are in the very same size regime, we do not understand the origin for this difference; possibly it is due to the higher degree of contamination in their (tap)-water as compared to the ultra-clean water in our case. It is hard to estimate the experimental

damping coefficient $\gamma_{\rm exp}$ of the shape oscillations from the axes dynamics such as in Figure 3. Comparing the first two peaks one gets $\gamma_{\rm exp} \approx 30$ s^{-1}. The corresponding theoretical value [19,22] is $\gamma_{\rm theory} = 56\ \nu^2/(3R) \approx 13$ s^{-1}.

5 Discussion and conclusions

In conclusion, we have performed experiments with 2–4 mm diameter bubbles interacting with a hot-film anemometer probe in ultra-clean water. The interaction can induce bubble shape oscillations. The main findings are:

- The experiments clearly show that the shape-oscillating bubbles after the interaction do not have higher mean velocities than the non-oscillating bubbles before the interaction, in contrast to Wu and Gharib [1], who measure much larger velocities for a shape oscillating bubble.
- The shape-oscillations result in an oscillating bubble rise velocity. It is shown through a simple force balance model that the (oscillating) added-mass force causes the oscillations in the velocity.

This second finding of course depends on the bubble diameter. If we compare estimates of the various forces in equation (10), we obtain

$$\frac{F_a}{F_d} \approx \frac{f\frac{1}{2}\rho_l\frac{4}{3}\pi R^3 v}{\frac{1}{2}C_d\rho_l\pi R^2 v^2} = \frac{\sqrt{6}}{36\pi}\sqrt{\frac{d\sigma}{\rho_l\nu^2}} = \frac{\sqrt{6}}{36\pi}\frac{Re}{\sqrt{We}}, \quad (12)$$

where $f = \omega_2/2\pi$ is the shape oscillation frequency following from equation (1), and

$$\frac{F_a}{F_b} = \frac{\frac{1}{2}\rho_l V_b v}{\rho_l V_b g} = \frac{\sqrt{6}}{\pi}\sqrt{\frac{\sigma}{\rho_l d^3}}\frac{v}{g} = \frac{\sqrt{6}}{\pi}\frac{Fr^2}{\sqrt{We}}, \quad (13)$$

where we have introduced the Froude number $Fr = v/\sqrt{gd}$. Indeed, for the 2.5 mm diameter bubble here we have $F_a/F_d \approx 9$, confirming the claim that the added mass force is dominant. However, for smaller bubbles the drag force will of course get more and more important. *E.g.* equal importance of drag and added mass occurs at $F_a/F_d = 1$, corresponding to a bubble with a diameter of $d \approx 216\pi^2\rho_l\nu^2/\sigma \approx 30\ \mu$m.

We thank A. Prosperetti, J. Magnaudet, and M. Wu for helpful discussions and comments and J. Rensen for help with the experimental setup. The work is part of the research program of FOM, which is financially supported by NWO, and J. de V. acknowledges financial support. S.L. acknowledges support from the European Union (EU) through the European Research Network on "Nonideal Turbulence" (contract HPRN–CT–200000162).

References

1. M. Wu, M. Gharib, Phys. Fluids **14**, L49 (2002)
2. R. Clift, J.R. Grace, M.E. Weber, *Bubbles, drops and particles* (Academics Press, New York, 1978)
3. P.C. Duineveld, J. Fluid Mech. **292**, 325 (1995)
4. R. Bel Fdhila, P.C. Duineveld, Phys. Fluids **8**, 310 (1996)
5. T. Maxworthy, C. Gnann, M. Kürten, F. Durst, J. Fluid Mech. **321**, 421 (1996)
6. A.W.G. de Vries, Ph.D. thesis, University of Twente, 2001
7. K. Lunde, R.J. Perkins, Appl. Sci. Res. **58**, 387 (1998)
8. K. Ellingsen, F. Risso, J. Fluid Mech. **440**, 235 (2001)
9. C. Brücker, Phys. Fluids **11**, 1781 (1999)
10. P.G. Saffman, J. Fluid Mech. **1**, 249 (1956)
11. G. Mougin, J. Magnaudet, Phys. Rev. Lett. **88**, 014502 (2002)
12. J. Magnaudet, I. Eames, Ann. Rev. Fluid Mech. **32**, 659 (2000)
13. J. Rensen, D. Bosman, J. Magnaudet, C.D. Ohl, A. Prosperetti, R. Toegel, M. Versluis, D. Lohse, Phys. Rev. Lett. **86**, 4819 (2001)
14. C.D. Ohl, A. Tijink, A. Prosperetti, J. Fluid Mech., in press
15. H.H. Bruun, *Hot wire anemometry: principles and signal analysis* (Oxford University Press, Oxford, 1995)
16. S. Luther, J. de Vries, J. Rensen, D. Lohse, preprint, Twente, 2002
17. R.E. Kalman, Transactions of ASME - J. Basic Eng. **82**, 35 (1960)
18. P.S. Maybeck, *Stochastic models, estimation, and control* (Academic Press, New York, 1979)
19. H. Lamb, *Hydrodynamics* (Cambridge University Press, Cambridge, 1932)
20. G.K. Batchelor, *An introduction to fluid dynamics* (Cambridge University Press, Cambridge, 1970)
21. D.W. Moore, J. Fluid Mech. **23**, 749 (1965)
22. M.P. Brenner, S. Hilgenfeldt, D. Lohse, Rev. Mod. Phys. **74**, 425 (2002)